PAPER

Double-layered micellar interpolyelectrolyte complexes—how many shells to a core?

Christopher V. Synatschke,[a] Felix H. Schacher,[*ab] Melanie Förtsch,[a] Markus Drechsler[a] and Axel H. E. Müller[*a]

We report on the formation of double-layered micellar interpolyelectrolyte complexes (IPECs) from ABC triblock terpolymer precursor micelles and hydrophilic homo- or block copolymers. Polybutadiene-*block*-poly(1-methyl-2-vinyl pyridinium)-*block*-poly(sodium methacrylate) (PB-*b*-P2VPq-*b*-PMANa) block terpolymers form micelles in aqueous solution at high pH exhibiting a PB core, a P2VPq/PMANa intramicellar IPEC (*im*-IPEC) shell, and a PMANa corona, which is negatively charged. Upon mixing with either positively charged, quaternized poly(N,N-dimethylaminoethyl methacrylate) (PDMAEMAq) homopolymers or its double-hydrophilic block copolymer with poly(ethylene oxide) (PEO-*b*-PDMAEMAq), a further IPEC shell is formed, rendering core–shell–shell–corona aggregates. The effects of the ratio of positive to negative charges, $Z_{+/-}$, the composition of the block terpolymer micelles, and the length of the added Dq block were investigated. We show that within a certain $Z_{+/-}$ regime stable complex micellar IPECs featuring two distinguishable IPEC shells are formed. The so-formed complex particles were analyzed by dynamic light scattering and cryogenic transmission electron microscopy.

Introduction

Self-assembly of block co- and terpolymers in solution has received considerable interest during the past decade.[1,2] Typically, such processes lead to the formation of spherical micelles,[3,4] cylindrical or rod-like aggregates,[5–7] or vesicles.[8] Particular interest is devoted to the control of size, size distribution, shape, or the number or type of functional groups present on the surface of such particles. This can be achieved by controlling the kinetics of the self-assembly process,[9] through changing the polymer composition or architecture,[10] or *via* the variation of external parameters like the employed solvent,[11,12] pH,[13] salinity,[14] or temperature.[15]

Another possibility to influence self-assembly processes in solution is to employ block copolymers with charged compartments, or polyelectrolyte segments.[16,17] Such polyelectrolytes can be natural (*e.g.*, polynucleic acids) or synthetic polyanions or -cations and can be further subdivided into weak (*e.g.*, poly-(methacrylic acid), PMAA) or strong (*e.g.*, poly(styrene sulfonate)) species.[18] Recent research interest in such materials has been primarily based on intrinsic properties such as water

solubility, very strong inter- and intra-chain interactions, ionic conductivity, and surface activity.[19]

Mixing of two different block copolymers with polyelectrolyte segments bearing opposite charges in aqueous solution leads to electrostatic co-assembly and the formation of interpolyelectrolyte complexes (IPECs).[20–22] The driving force is the entropy gain from the release of the counterions. Such IPECs are hydrophobic yet are still able to participate in dynamic polyion exchange reactions in aqueous media.[23,24] If weak polyelectrolytes like PMAA are used, the complex formation is pH-dependent.[25] In addition, the IPEC formation is reversible: the addition of large amounts of salt leads to a screening of the charges and to a breakup of the complexes.[20,26] If preformed micelles with a charged corona are mixed with oppositely charged polyelectrolytes, an elegant route towards complex micellar architectures is opened. This has been demonstrated for micelles exhibiting a soft polyisobutylene core and a PMAA corona[25,26] or for more complex core-compartmentalized block terpolymer micelles.[27]

Within this contribution we demonstrate for the first time the formation of two distinctly different adjacent IPEC shells within the same complex micellar aggregate. As starting material we employ multicompartment micelles exhibiting a soft polybutadiene (PB) core, a discontinuous shell consisting of an intramicellar IPEC (*im*-IPEC) between quaternized poly(2-vinyl pyridine) (P2VPq) and poly(sodium methacrylate) (PMANa), and a corona of excess PMANa, thus rendering colloidal objects with a negative surface charge. These micelles are formed if

[a] Makromolekulare Chemie II und Bayreuther Zentrum für Kolloide und Grenzflächen, Universität Bayreuth, D-95440 Bayreuth, Germany. E-mail: axel.mueller@uni-bayreuth.de
[b] Institut für Organische Chemie und Makromolekulare Chemie, Friedrich-Schiller-Universität Jena, D-07743 Jena, Germany. E-mail: felix.schacher@uni-jena.de

ampholytic block terpolymers, polybutadiene-*block*-poly-(1-methyl-2-vinyl pyridinium)-*block*-poly(sodium methacrylate) (PB-*b*-P2VPq-*b*-PMANa), self-assemble in aqueous solution at pH 10; conditions where methacrylic acid is negatively charged.[28] To this is added another solution containing a positively charged polyelectrolyte, being either quaternized poly(*N*,*N*-dimethylaminoethyl methacrylate) (PDMAEMAq) homopolymers of different chain lengths or the corresponding double-hydrophilic block copolymer with poly(ethylene oxide) (PEO-*b*-PDMAEMAq). This then results in further IPEC formation between the PMANa corona and PDMAEMAq and the generation of a second IPEC shell. The whole process is shown in Scheme 1.

In the case of PEO-*b*-PDMAEMAq, the PEO chains then serve as the corona of the generated core–shell–shell–corona particle and maintain a good solubility in aqueous media. We investigated two PDMAEMAq homopolymers of different chain lengths, in short: Dq_{162} and Dq_{820}, and one double-hydrophilic block copolymer, $EO_{325}Dq_{157}$, the subscripts denoting the degree of polymerization of the corresponding block. As precursor micelles three different block terpolymers, PB_{800}-*b*-$P2VPq_{190}$-*b*-$PMANa_{345}$, PB_{800}-*b*-$P2VPq_{190}$-*b*-$PMANa_{465}$, and PB_{800}-*b*-$P2VPq_{190}$-*b*-$PMANa_{550}$, were used. In the following sections a shorter nomenclature, $BVqMANa_x$, will be used for the precursor micelles, as the first two blocks (B and Vq) have the same degree of polymerization in all cases shown in this manuscript. The complexations were performed at different $Z_{+/-}$ values. We define $Z_{+/-}$ by dividing the number of cationic Dq monomer units added to the micellar solution divided by the number of free (non-complexed) anionic MANa units present, as shown in eqn (1).

$$Z_{+/-} = \frac{n_{Dq}}{n_{MANa} - n_{Vq}} \quad (1)$$

The structure and the stability of the formed micellar IPECs were analyzed using dynamic light scattering (DLS) and cyrogenic transmission electron microscopy (cryo-TEM).

Experimental

Synthesis

Materials. The solvents for the preparation of the micellar solutions were purchased in p.a. grade and used as delivered. Dimethyl sulfate (Me_2SO_4, >99%, Aldrich) and hydrochloric acid (32%) were used as received. Buffer solutions with pH 10 (H_3BO_3/KCl/NaOH) were obtained from Fluka and contained about 0.3 wt% salt. The initiator for ATRP, ethylbromoisobutyrate (EBIB) was distilled and stored under nitrogen. HMTETA was distilled prior to use. Anisole (p.a. grade, Fluka) and CuBr (>99%, Aldrich) were used as received.

Synthesis of the PB-*b*-P2VP-*b*-P*t*BMA block terpolymers. The linear block terpolymers were synthesized *via* sequential living anionic polymerization in THF at low temperatures using *sec*-butyllithium as an initiator. A detailed description of the synthetic procedure and a comprehensive investigation of PB-*b*-P2VP-*b*-P*t*BMA block terpolymers with different volume fractions are reported elsewhere.[29]

Synthesis of PEO-*b*-PDMAEMA ($EO_{325}D_{157}$). EO-*b*-D was prepared *via* sequential living anionic polymerization in THF using 1,1-diphenyl-3-methylpentyllithium (DPMPLi) as initiator. A combination of MALDI-ToF mass spectrometry and ^{1}H-NMR yielded the composition $EO_{325}D_{157}$. More details about the synthesis and characterization can be found elsewhere.[30]

Synthesis of PDMAEMA (D_{162} and D_{820}). D_{162} was prepared with Atom Transfer Radical Polymerization (ATRP) in anisole using an earlier reported protocol.[31] The ratio of monomer to initiator was 500 : 1 and the reaction was quenched at ~40% conversion (followed by ^{1}H-NMR). D_{162} has a molecular weight of $M_{NMR} = 25.500$ g mol^{-1} and a PDI of 1.26, measured with
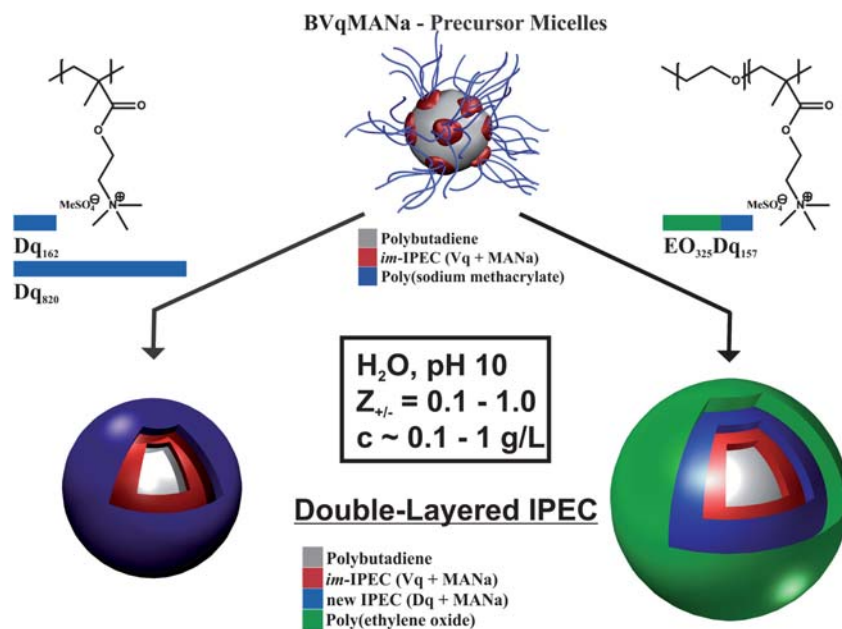
Scheme 1 Schematic pathway for the formation of double-layered IPECs from PB-*b*-P2VPq-*b*-PMANa block terpolymer micelles and either PDMAEMAq homopolymers (left) or a PEO-*b*-PDMAEMAq diblock copolymer (right).

THF-SEC with additional 0.25 wt% tetrabutyl ammonium bromide (TBAB). Polystyrene standards were used for calibration ($M_{\text{n,SEC}}$ = 29.300 g mol^{-1}). The ATRP of D$_{820}$ was accomplished in acetone at 60 °C. The ratio of initiator : CuBr : HMTETA : monomer was 1 : 4 : 4 : 1200 and the polymerization was stopped at a conversion of 68% as determined by NMR. The polymer exhibited a molecular weight M_{NMR} = 130.000 g mol^{-1} and a PDI of 1.51.

Quaternization of the P2VP block. PB-*b*-P2VP-*b*-P*t*BMA block terpolymers were dissolved in dioxane at a concentration of 1 g L^{-1}. Afterwards, Me$_2$SO$_4$ (10 eq. corresponding to the 2-vinyl pyridine groups) was added and the solution was stirred for at least 72 hours at 40 °C. The resulting solution of poly-butadiene-*block*-poly(*N*-methyl-2-vinyl pyridinium)-*block*-poly-(*tert*-butyl methacrylate) PB-*b*-P2VPq-*b*-P*t*BMA was directly used for the subsequent hydrolysis of the ester moiety of the P*t*BMA block. From IR measurements and iodometric titrations with diluted AgNO$_3$ solutions we determined an approximate degree of quaternization of 70–90%. The quaternization of D or the EO-*b*-D diblock copolymer was performed in an analogous way. Here, a quantitative quaternization was achieved as proven by ^{1}H-NMR spectroscopy.[31]

Dialysis. Dialysis membrane tubing (MWCO 3.500 g mol^{-1}, regenerated cellulose ester) was purchased from Spectra/Por. Prior to use, the tubes were immersed in de-ionized water for 1 h to open the pores.

Hydrolysis of the P*t*BMA block. Solutions of PB-*b*-P2VPq-*b*-P*t*BMA in dioxane (c = 1 g L^{-1}) were treated with a 5-fold excess of hydrochloric acid relative to the ester moieties. Afterwards, the reaction mixture was refluxed at 120 °C for 24 hours. Full conversion of the hydrolysis reaction was confirmed with IR spectroscopy *via* the disappearance of the *tert*-butyl (1393 cm^{-1} and 1367 cm^{-1}) and carbonyl (1722 cm^{-1}) signals.

Preparation of the PB-*b*-P2VPq-*b*-PMANa (BVqMANa) micellar solutions. Directly after hydrolysis of the P*t*BMA block, micellar stock solutions (c ≈ 1 g L^{-1}) were prepared *via* dialysis against pH 10 buffer solution.

Complexation reactions. Dq$_{167}$, Dq$_{820}$ and EO$_{325}$Dq$_{157}$ were dissolved in a pH 10 buffer solution at a respective concentration of 5 g L^{-1}. Afterwards, the corresponding volumes to reach a certain $Z_{+/-}$-value (for the definition of $Z_{+/-}$ see the Introduction) were added to micellar solutions of BVqMANa$_{345}$, BVqMANa$_{465}$, or BVqMANa$_{550}$ (all 1 g L^{-1}) in small glass vials and stirred at ambient temperature. In general, measurements on the complexes were performed after one week of continuous stirring.

Characterization

Dynamic light scattering (DLS). All experiments were performed using approximately the same concentrations (c = 1 g L^{-1}). DLS measurements were performed in sealed cylindrical scattering cells (d = 10 mm) at an angle of 90° on an ALV DLS/SLS-SP 5022F equipment consisting of an ALV-SP 125 laser goniometer with an ALV 5000/E correlator and a He–Ne laser with the wavelength λ = 632.8 nm. The CONTIN algorithm was applied to analyze the obtained correlation functions. Apparent hydrodynamic radii were calculated according to the Stokes–Einstein equation. Prior to the light scattering measurements the sample solutions were filtered using Millipore nylon filters with a pore size of 1.2 (solutions of the quaternized Dq$_{162}$, Dq$_{820}$, or the double-hydrophilic EO$_{325}$Dq$_{157}$ in pH 10 buffer) or 5 μm (micellar precursors or the double-layered IPECs). The polydispersities were determined from unimodal peaks *via* the cumulant analysis.

Cryogenic transmission electron microscopy (cryo-TEM). For cryo-TEM studies, a drop of the sample solution (c ≈ 0.1 wt%, 1 g L^{-1}) was placed on a lacey carbon-coated copper TEM grid (200 mesh, Science Services, München, Germany), where most of the liquid was removed with blotting paper, leaving a thin film stretched over the grid holes. The specimens were shock vitrified by rapid immersion into liquid ethane in a temperature-controlled freezing unit (Zeiss Cryobox, Zeiss NTS GmbH, Oberkochen, Germany) and cooled to approximately 100 K. The temperature was monitored and kept constant in the chamber during all the preparation steps. After freezing the specimens, they were inserted into a cryo-transfer holder (CT3500, Gatan, München, Germany) and transferred to a Zeiss EM922 Omega EFTEM instrument. Examinations were carried out at temperatures around 100 K. The microscope was operated at an acceleration voltage of 200 kV. Zero-loss filtered images (ΔE = 0 eV) were taken under reduced dose conditions. All images were registered digitally by a bottom mounted CCD camera system (Ultrascan 1000, Gatan), combined and processed with a digital imaging processing system (Gatan Digital Micrograph 3.9 for GMS 1.4).

ζ-Potential. The ζ-potential was determined on a Malvern Zetasizer Nano ZS in conjunction with an MPT2 autotitrator (Malvern). The electrophoretic mobilities (u) were converted into ζ potentials *via* the Smoluchowski equation $\zeta = u\eta/\varepsilon_0\varepsilon$, where η denotes the viscosity and $\varepsilon_0\varepsilon$ the permittivity of the solvent, water.

Size exclusion chromatography (SEC). Four PSS–SDV gel columns (5 μm) with a porosity range from 10^2 to 10^5 Å (PSS, Mainz, Germany) were used together with a differential refractometer and a UV detector at λ = 254 nm. Measurements were performed in THF with a flow rate of 1 mL min^{-1} using toluene as internal standard. Narrowly distributed 1,4-polybutadiene were used as calibration standards.

SEC experiments for the PDMAEMA containing samples were performed using four PSS–SDV gel columns (5 μm) with a porosity range from 10^2 to 10^4 Å (PSS, Mainz, Germany) together with a differential refractometer and a UV detector at λ = 254 nm. Measurements were performed in THF with additional 0.25 wt% tetrabutylammonium bromide (TBAB) as eluent and 0.5 mL min^{-1} as flow rate. Polystyrene standards were used for calibration.

^{1}H-NMR spectroscopy. The absolute number-average molecular weights, M_n, of the synthesized block copolymers were

determined by ^{1}H-NMR in CDCl$_3$ (Bruker AC 250 spectrometer) using the M_n of the first block, as determined by MALDI-ToF MS or SEC, and suitable NMR signal areas of the corresponding blocks. For more details on the characterization of the block copolymers the reader is referred to the literature.[32]

Results and discussion

Characterization of the precursor micelles

In a recent publication we reported on the preparation of multicompartment-core micelles in aqueous media at high pH from polybutadiene-*block*-poly(1-methyl-2-vinyl pyridinium)-*block*-poly(sodium methacrylate) (BVqMANa) block terpolymers.[28] The micelles consisted of a soft B core, a discontinuous shell of an intramicellar IPEC (*im*-IPEC) between positively charged Vq and negatively charged poly(sodium methacrylate) (MANa at pH 10), and, depending on the length, a corona of MANa. They were shown to react on changes in pH and salinity in a dynamic way. These micelles were used as "precursor" materials for the results presented within this contribution. Three block terpolymer compositions were used. The first two blocks, B and Vq, are of the same length for all three polymers, while the length of the MANa block was varied. The solution characteristics of the precursor micelles in pH 10 buffer solution were determined by cryo-TEM, DLS and ζ-potential measurements (see Table 1).

Representative cryo-TEM images of the precursor micelles 1–3 are shown in Fig. 1, where the proposed solution structure of multicompartment micelles can be confirmed. The BVqMANa$_x$ polymers form micelles with a B core (dark grey), which is decorated with the *im*-IPEC consisting of Vq and MANa (small black dots), and a corona of the remaining MANa (light grey). With increasing length of the MANa block, the micelles appear more homogeneous in size and shape. Several micelles for BVqMANa$_{345}$ exhibit a non-spherical shape, especially the core of the micelles shows deformations (see Fig. 1A), whereas this cannot be seen for polymers with a longer water-soluble block (Fig. 1B and C). Furthermore, some of the BVqMANa$_{345}$ micelles seem to be interconnected by bridge-like structures (dark grey, shown at higher magnification in the inset of Fig. 1A). Similar structures were previously observed in micellar systems prepared from amphiphilic miktoarm stars of polystyrene-*arm*-polybutadiene-*arm*-poly(2-vinyl pyridine) (μSBV) block terpolymers in aqueous media and identified as hydrophobic B bridges, originating from the soft "liquid" cores of the aggregates.[33] For both BVqMANa$_{465}$ and BVqMANa$_{550}$, such effects

Table 1 Molecular characterization of the BVqMANa$_x$ block terpolymers and the micellar aggregates in aqueous solution at pH 10

Polymer	Composition^a	$10^{-3} M_n{}^b$/g mol^{-1}	$\langle R_{TEM}\rangle_n{}^c$/nm	$\langle R_h\rangle_{z,app.}{}^d$/nm	PDI$_{app.}{}^e$	ζ-Potential/mV
1	B$_{800}$Vq$_{190}$MANa$_{345}$	96	79.$_5$ ± 7	170	0.18	−21
2	B$_{800}$Vq$_{190}$MANa$_{465}$	106	93.$_5$ ± 8	146	0.21	−30
3	B$_{800}$Vq$_{190}$MANa$_{550}$	113	91 ± 11	88	0.05	−36

^{a} The subscripts denote the respective degrees of polymerization. ^{b} Calculated for the individual polymer chain without taking the counterions into account. ^{c} Determined from cryo-TEM images. ^{d} Determined *via* DLS at 0.17 and 1 g L^{-1}. ^{e} Determined *via* cumulant analysis.
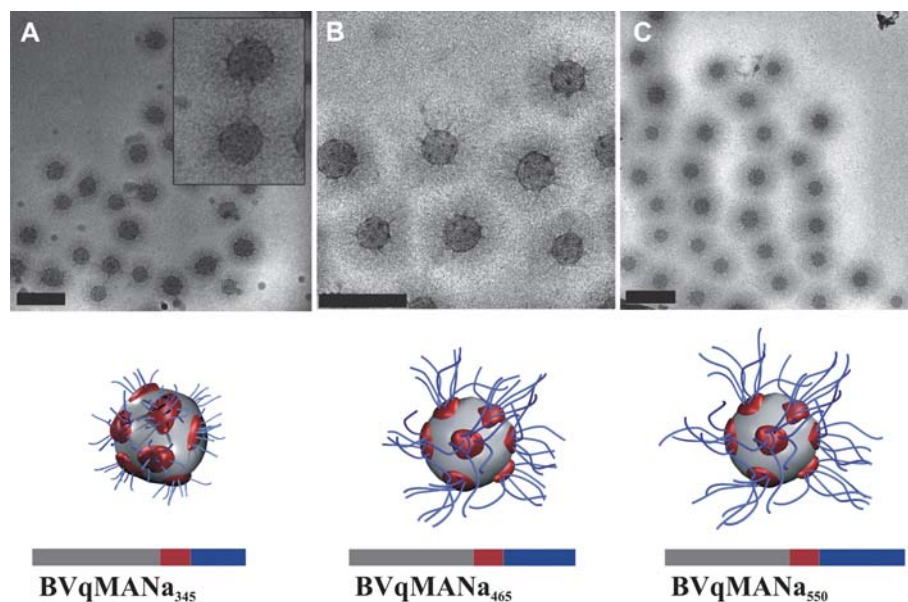

Fig. 1 Cryo-TEM images of micelles formed from BVqMANa$_{345}$ (A, the inset shows hydrophobic bridges between two adjacent micelles at higher magnification), BVqMANa$_{465}$ (B), and BVqMANa$_{550}$ (C) at concentrations of 1 g L^{-1} in aqueous solution at pH 10, all scale bars correspond to 200 nm; below each cryo-TEM image are schematic depictions of the proposed solution structure.

Table 2 Average sizes of the individual compartments of the BVqMA-Na$_x$ micelles as determined by image analysis of cryo-TEM data

Compartment	BVqMANa$_{345}$/nm	BVqMANa$_{465}$/nm	BVqMANa$_{550}$/nm
R_{Micelle}	79.5 ± 7	93.5 ± 8	91 ± 11
R_{Core}	38 ± 5	37 ± 8	33.5 ± 4
$D_{im\text{-IPEC}}$	5 ± 2	3 ± 1	4 ± 1
D_{Corona}	40 ± 5	52 ± 6	53 ± 9
$N_{\text{agg.}}{}^{a}$	3200	3000	2200

^{a} Estimated with eqn (2).

were not observed. We attribute this to a superior stabilization of the micelles in aqueous solution with an increasing block length of the corona-forming block, MANa.

The cryo-TEM images were subjected to a detailed image analysis to obtain average sizes of the individual compartments. For each micelle and compartment (core, im-IPEC and corona) between 50 and 100 micelles were measured to calculate average values (Table 2).

The smallest micelles are formed for BVqMANa$_{345}$ with an overall radius of 79.5 nm (Table 2), whereas both the aggregates found for BVqMANa$_{465}$ (93.5 nm) and BVqMANa$_{550}$ (91 nm) are larger. The diameter of the corona also increases with increasing length of the MANa block. The size of the im-IPEC stays constant at approximately 3–4 nm within the experimental error for all three samples discussed. However, the core radius seems to decrease with increasing length of the negatively charged block from 38 nm for BVqMANa$_{345}$ to 33.5 nm for BVqMANa$_{550}$, which points to a decrease in the aggregation number, $N_{\text{agg.}}$. This is in accordance with Burkhardt et al.,[3] who observed a decrease in $N_{\text{agg.}}$ with increasing hydrophilic block length in polyisobutylene-block-poly(methacrylic acid) micelles. They explained the decrease of $N_{\text{agg.}}$ with the increasing space occupied by the hydrophilic block leading to a repulsive force between the corona chains. Such a decrease in $N_{\text{agg.}}$ was also predicted by Borisov and Zhulina in theoretical calculations for diblock-copolymer micelles with one ionic block.[34] A rough calculation of $N_{\text{agg.}}$ for our system based on the core diameter as observed in TEM (eqn (2)) results in an approximate $N_{\text{agg.}}$ of 3200, 3000 and 2200 for BVqMANa$_{345}$, BVqMANa$_{465}$ and BVqMANa$_{550}$, respectively. We note that earlier static light scattering experiments on BVqMANa$_{550}$ gave a significantly lower value ($N_{\text{agg.}} = 234$) and that we are not able to explain this discrepancy at the moment.[28]

$$N_{\text{agg.}} = \frac{m_{\text{core}}}{m_{\text{PB}}^{\text{chain}}} = \frac{4\pi N_A \rho_{\text{PB}} R_{\text{core}}^3}{3 M_{\text{PB}}^{\text{chain}}} \quad (2)$$

with m_{core}: mass of the micellar core; $m_{\text{PB}}^{\text{chain}}$: mass of an individual PB chain; N_A: Avogadro constant; ρ_{PB}: density of polybutadiene; R_{core}: radius of the micellar core according to TEM; $M_{\text{PB}}^{\text{chain}}$: molecular weight of an individual PB chain.

If the aggregate sizes determined via cryo-TEM are compared to the data obtained from DLS measurements (Table 1), deviations are found for BVqMANa$_{345}$ and BVqMANa$_{465}$, whereas in the case of BVqMANa$_{550}$ both methods are in good agreement. According to cryo-TEM (Table 2, Fig. 1), BVqMANa$_{345}$ has an $\langle R_{\text{TEM}} \rangle_n = 79.5$ nm, while DLS experiments yield $\langle R_{\text{h}} \rangle_{z,\text{app.}} = 170$ nm and a PDI of 0.18. We think that this difference can be

tentatively explained by the bridges observed (inset in Fig. 1A), masking the individual aggregate size. The reason for the difference in R for BVqMANa$_{465}$ (DLS: $\langle R_{\text{h}} \rangle_{z,\text{app.}}$, = 146 nm, PDI = 0.21 and cryo-TEM: $\langle R_{\text{TEM}} \rangle_n = 93.5$ nm) remains puzzling. In this case, hydrophobic bridges were not observed in cryo-TEM. Nevertheless, the increased value obtained by DLS might still hint towards aggregation of the micelles taking place in the stock solution. Furthermore, the values for R obtained via cryo-TEM represent a number average, whereas DLS gives a z-average. Especially for systems with higher PDI values, the differences between these two averages are expected to be significant.

Complexation and IPEC formation

To generate an additional IPEC layer on top of the already existing im-IPEC shell, the BVqMANa$_x$ micelles were mixed with positively charged polyelectrolytes in aqueous solution at pH 10. We have demonstrated this approach recently for the addition of poly(ethylene oxide)-block-poly(1-methyl-2-vinyl pyridinium) PEO-b-P2VPq diblock copolymers.[27] In this case, two identical IPEC shells were formed as both the "inner", former im-IPEC, as well as the "outer", newly generated IPEC, consisted of Vq and MANa. Here, we employed either quaternized PDMAEMA (Dq) or PEO-b-PDMAEMAq diblock copolymers as oppositely charged polyelectrolytes. The whole process is depicted in Scheme 1.

If cationic homopolymers (Dq$_{162}$, Dq$_{820}$) are used for further IPEC formation (Scheme 1, left part), core–shell–shell particles are formed where the previous MANa corona of the micelles is transformed into an IPEC layer consisting of MANa and Dq. Furthermore, the two IPECs are expected to form two distinctive layers due to immiscibility between Vq and Dq. Depending on the absolute ratio of positive to negative charges, $Z_{+/-}$, this would lead to uncharged polymer particles. It has been shown that such IPECs precipitate when a critical $Z_{+/-}$ value is reached.[26] If EO$_{325}$Dq$_{157}$ is used for this complexation step, core–shell–shell–corona particles are formed. In this case, even for $Z_{+/-} = 1$, the micellar IPECs are expected to remain water-soluble, stabilized through the PEO corona, depicted in green (Scheme 1, right part).

We will first discuss the results concerning the IPEC-formation of different BVqMANa$_x$ precursor micelles with Dq$_{162}$ or Dq$_{820}$ at different $Z_{+/-}$ values. Afterwards, similar experiments will be discussed with EO$_{325}$Dq$_{157}$. Unless explicitly stated, the concentration of the precursor micelles was in between 0.1 and 1.0 g L^{-1} in pH 10 buffer solutions for the complexation reactions, a regime proven not to lead to further aggregation for BVqMANa$_{550}$.[28] However, in the case of BVqMANa$_{345}$ and BVqMANa$_{465}$, a slight increase in hydrodynamic radius was observed with concentration ($\langle R_{\text{h}} \rangle_{z,\text{app.}} = 172$ nm for 0.17 g L^{-1} and $\langle R_{\text{h}} \rangle_{z,\text{app.}} = 195$ nm for 1.0 g L^{-1} for BVqMANa$_{345}$ and $\langle R_{\text{h}} \rangle_{z,\text{app.}} = 146$ nm for 0.17 g L^{-1} and $\langle R_{\text{h}} \rangle_{z,\text{app.}} = 191$ for 1 g L^{-1} for BVqMANa$_{465}$). Therefore, those were typically used at 0.17 g L^{-1}. The targeted amounts of quaternized homo- or diblock copolymers were added at a concentration of 5 g L^{-1} prepared in the same pH 10 buffer. The highest resulting polymer concentration prepared in that way (solutions of 1.0 g L^{-1} BVqMANa$_{550}$ micelles with EO$_{325}$Dq$_{157}$ at $Z_{+/-} = 1$) was
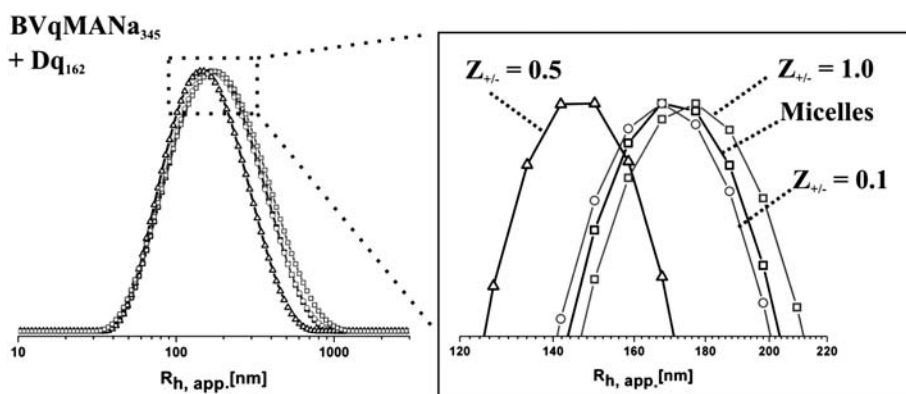
Fig. 2 DLS CONTIN plots for $BVqMANa_{345}$ (-□-, black), and micellar IPECs with Dq_{162} at $Z_{+/-} = 0.1$ (-○-, grey), 0.5 (-△-, black) and 1.0 (-□-, grey) (A), the inset on the right shows an enlargement of the plot peak region.

roughly 1.7 g L^{-1}. The cationic homo- or diblock copolymer solution was added under vigorous stirring to the solution containing the precursor micelles. In general, the resulting micellar IPECs were examined after one week of continuous stirring.

Addition of Dq homopolymers to $BVqMANa_x$ micelles

$BVqMANa_x$ precursor micelles were mixed with Dq_{162} or Dq_{820} at different $Z_{+/-}$ ratios and analyzed by DLS. Exemplarily, the resulting CONTIN plots for $BVqMANa_{345}$ and Dq_{162} at different $Z_{+/-}$ ratios are shown in Fig. 2, while the results for all different combinations are summarized in Table 3.

For all possible combinations of $BVqMANa_x$ block terpolymer micelles and Dq homopolymers critical $Z_{+/-}$ ratios,

above which precipitation of the complexes occurred within several hours, were found. Interestingly, as can be seen from Table 3, the critical $Z_{+/-}$ value decreases with increasing MANa block length. $BVqMANa_{345}$ micelles tolerated an addition of Dq polymers up to $Z_{+/-} = 1$, whereas for $BVqMANa_{550}$ precipitation already occurred at $Z_{+/-} = 0.5$, which is rather puzzling.

Remarkable differences are also observed if the hydrodynamic radii of the micellar IPECs after addition of oppositely charged Dq are compared: for $BVqMANa_{345}$ and $BVqMANa_{465}$, the micellar size does not significantly change if small amounts ($Z_{+/-} < 0.25$ for $BVqMANa_{345}$ and $Z_{+/-} < 0.5$ for $BVqMANa_{465}$) of Dq_{162} are added. Upon further addition of Dq_{162} the size increases until a critical $Z_{+/-}$ value is reached, where aggregation and finally precipitation occur ($Z_{+/-} = 1.25$ for $BVqMANa_{345}$ and $Z_{+/-} = 1.0$ for $BVqMANa_{465}$). For $BVqMANa_{550}$, already the addition of 10% of Dq_{162} causes an increase in R_h from 88 nm to 169 nm. Increasing the $Z_{+/-}$ to 0.25 leads to a decrease in size of the micellar IPECs, before precipitation occurs at the critical $Z_{+/-}$ value of 0.5.

In theory, Dq_{162} can interact with the negatively charged MANa corona in two possible ways: if all MANa chains of the corona are evenly neutralized, a collapse of the corona should occur. On the other hand, if only some MANa chains are fully neutralized and participate in the IPEC formation, the other uncomplexed MANa chains would retain their original length. This would lead to a less drastic change in corona size. This question was investigated by Borisov et al. in a recent publication, where molecular dynamics simulations on the structural organization of IPECs between oppositely charged linear and star-shaped polyelectrolytes were performed.[35] They found that for star-shaped polyelectrolytes several arms were completely neutralized whilst others did not participate at all in the IPEC formation. A similar behavior was also found for small amounts of surfactant added to spherical polyelectrolyte brushes.[36] We assume that a similar mechanism is taking place here. This would explain the absence of significant changes in R_h for small $Z_{+/-}$ values in the case of micellar IPEC formation for $BVqMANa_{345}$ and $BVqMANa_{465}$ with Dq_{162}. If larger amounts of Dq_{162} are added, a drastic increase in the size of the structures indicates the formation of aggregates. This is simply caused through less and less "free" MANa being present to stabilize the particles in solution, until, finally, the aggregates precipitate.

Table 3 Apparent hydrodynamic radii of double-layered micellar IPECs prepared from $BVqMANa_x$ block terpolymer micelles and Dq polymers as determined by DLS

Entry	Sample	$Z_{+/-}$[a]	$\langle R_h \rangle_{z,app.}$[b]/nm	PDI[c]
1	$BVqMANa_{345}$	—	170	0.18
2	$BVqMANa_{345} + Dq_{162}$	0.1	172	0.27
3	$BVqMANa_{345} + Dq_{162}$	0.5	154	0.24
4	$BVqMANa_{345} + Dq_{162}$	1.0	184	0.34
5	$BVqMANa_{345} + Dq_{162}$	1.25	Precipitation	
6	$BVqMANa_{345} + Dq_{820}$	0.5	162	0.27
7	$BVqMANa_{345} + Dq_{820}$	1.0	186	0.27
8	$BVqMANa_{465}$	—	146	0.21
9	$BVqMANa_{465} + Dq_{162}$	0.1	145	0.18
10	$BVqMANa_{465} + Dq_{162}$	0.5	148	0.21
11	$BVqMANa_{465} + Dq_{162}$	0.75	170	0.25
12	$BVqMANa_{465} + Dq_{162}$	1.0	Precipitation	
13	$BVqMANa_{465} + Dq_{820}$	0.1	115	0.12
14	$BVqMANa_{465} + Dq_{820}$	0.5	181	0.21
15	$BVqMANa_{465} + Dq_{820}$	0.75	Precipitation	
16	$BVqMANa_{550}$	—	88	0.05
17	$BVqMANa_{550} + Dq_{162}$	0.1	169	0.16
18	$BVqMANa_{550} + Dq_{162}$	0.25	128	0.17
19	$BVqMANa_{550} + Dq_{162}$	0.5	Precipitation	
20	$BVqMANa_{550} + Dq_{820}$	0.1	110	0.13
21	$BVqMANa_{550} + Dq_{820}$	0.25	131	0.09
22	$BVqMANa_{550} + Dq_{820}$	0.5	Precipitation	

[a] Ratio of added positive to remaining negative charges. [b] Determined via DLS. [c] Determined via cumulant analysis.

If a longer cationic polyelectrolyte, Dq_{820}, is used for the complexation reactions, the situation is different. For small $Z_{+/-}$ values (0.1), a slight contraction of the micellar IPECs for $BVqMANa_{345}$ and $BVqMANa_{465}$ can be seen (Table 3, entries 6 and 13), while $BVqMANa_{550}$ complexes again show an increase in R_h (Table 3, entry 20). A tentative explanation for the differences observed for $BVqMANa_{550}$ could be that with increasing MANa block length (and a longer polycationic chain, Dq_{820}) *inter*-micellar linkages are also formed to a certain extent. As shown for Dq_{162}, the addition of more Dq_{820} eventually exceeds a critical $Z_{+/-}$ value in all cases and results in precipitation of the formed complexes. Considering the PDI of the resulting aggregates (according to DLS), in most cases the addition of Dq polymers leads to an increase for the complex micelles (exceptions are $BVqMAA_{465}$ micelles, entries 9 and 13 in Table 3). In general, the highest PDIs are observed for high $Z_{+/-}$ ratios, shortly before precipitation occurs. This observation is reasonable, as increasing complexation of the corona should result in poorly stabilized micelles, which in turn promotes aggregation and broadens the micellar size distribution. Even though both Dq polymers are moderately polydisperse (PDI(Dq_{162}) = 1.26; PDI(Dq_{820}) = 1.51), the effect of the $Z_{+/-}$ ratio seems to be more pronounced. This is in accordance with earlier work on star-shaped poly(acrylic acid) complexes with quaternized P4VPq homopolymers.[37]

For a validation of a successful complexation and, hence, the formation of a second IPEC shell, cryo-TEM was performed for the complexes prepared from all $BVqMANa_x$ block terpolymer micelles and the longer Dq_{820} polycation. The results are shown in Fig. 3.

The cryo-TEM images confirm the proposed core–shell–shell morphology of the complexes. Throughout all the samples, but especially for the complexes of $BVqMANa_{550}$ with Dq, highly aggregated particles were found in the cryo-TEM samples. This implicates that, although low $Z_{+/-}$ values are used, the particles are not significantly charged and do not repel each other anymore. The increase in R_h that is observed in the DLS for large $Z_{+/-}$ values could therefore be explained by clustering. One has to keep in mind, however, that in the cryo-TEM images a two-dimensional confinement of the particles takes place, which might further promote clustering of the particles. Moreover, a few precursor-like micelles were found for complexes of $BVqMANa_{345}$ (inset in Fig. 3A) and $BVqMANa_{465}$ with Dq_{820} at $Z_{+/-} = 0.5$. Some of these are depicted in the upper left corner of Fig. 3A one is also shown on the right-hand side of Fig. 3E. Such "precursor" micelles rather were an exception and we believe that these are a result of slow mixing during the addition of the Dq solutions.

The enlarged images in Fig. 3D and E nicely show the double-layered character of the micellar IPECs when compared to the original micelles. The grey B core is still surrounded by a thin, slightly darker shell. This is supposed to be the former discontinuous *im*-IPEC shell of the precursor micelles, consisting of Vq and MANa. Completely covering this part, a new continuous shell has been formed through the complexation of the MANa corona with Dq_{820}, depicted in blue in Fig. 3F. Again, the overall size of the micelles as well as the size of the individual compartments was determined from the cryo-TEM images for complexes of $BVqMANa_{345}$ and $BVqMANa_{465}$ with Dq_{820} and a $Z_{+/-}$ ratio of 0.5. The averaged values from counting 50–100 particles in each case together with the corresponding standard deviations are shown in Table 4. Unfortunately, in the case of micellar IPECs formed from $BVqMANa_{550}$ precursor micelles a detailed evaluation was not possible, due to the strong aggregation observed in the cryo-TEM images. Nevertheless, those solutions were stable over months.

If the overall radius is calculated according to the cryo-TEM micrographs by assuming it to be equal to half the core-to-core
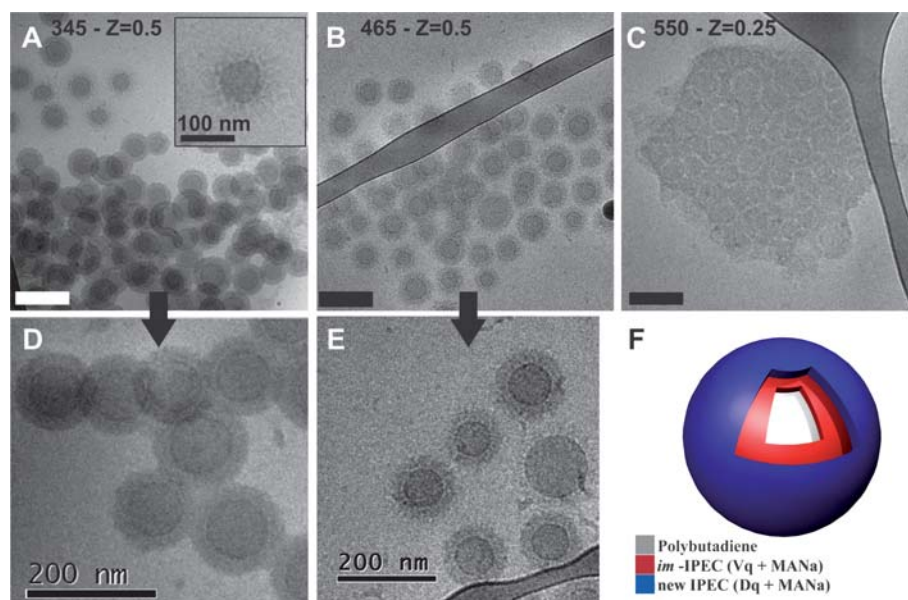

Fig. 3 Cryo-TEM micrographs of complexes formed from precursor micelles and Dq_{820} at different $Z_{+/-}$ ratios; $BVqMANa_{345}$ at $Z_{+/-} = 0.5$ (A, the inset shows a single precursor micelle, D shows a higher magnification); $BVqMANa_{465}$ at $Z_{+/-} = 0.5$ (B, E shows a higher magnification); $BVqMANa_{550}$ at $Z_{+/-} = 0.25$ (C); proposed solution structure of the resulting double-layered micellar IPECs (F); all scale bars correspond to 200 nm.

Table 4 Average compartment dimensions for micellar IPECs from BVqMANa$_x$/Dq$_{820}$ as determined by analysis of 50–100 particles

Compartment	BVqMANa$_{345}$/nm	BVqMANa$_{345}$/Dq$_{820}$ ($Z_{+/-} = 0.5$)/nm	BVqMANa$_{465}$/nm	BVqMANa$_{465}$/Dq$_{820}$ ($Z_{+/-} = 0.5$)/nm
R_{Micelle}	79.5 ± 7	65 ± 7	93.5 ± 8	61 ± 7
R_{Core}	38 ± 5	34.5 ± 5	37 ± 8	31 ± 4
$D_{im\text{-IPEC}}$	5 ± 2	8 ± 2	3 ± 1	6 ± 2
$D_{\text{corona/2}^{\text{nd}}\text{ IPEC-shell}}$	40 ± 5	23 ± 3	52 ± 6	25 ± 4
$N_{\text{agg.}}{}^a$	3200	2400	3000	1700

^{a} Estimated with eqn (2).

distance, a number-average $\langle R_{\text{TEM}} \rangle_n = 65$ nm for BVqMANa$_{345}$ and $\langle R_{\text{TEM}} \rangle_n = 61$ nm for BVqMANa$_{465}$ complexes is found (both were formed with Dq$_{820}$ at $Z_{+/-} = 0.5$, samples shown in Fig. 3). This is again distinctly smaller than the size observed *via* DLS, where $\langle R_{\text{h}} \rangle_{z,\text{app.}} = 162$ nm and $\langle R_{\text{h}} \rangle_{z,\text{app.}} = 181$ nm were determined. This discrepancy between both methods, to our opinion, reflects the tendency of these particles to aggregate after formation of the second IPEC shell, as also seen in some of the cryo-TEM images. Nevertheless, this did not seem to affect the stability of the micellar IPEC solutions. As a general observation from cryo-TEM, the overall size of the micelles seems to decrease after formation of the complexes with Dq$_{820}$. This decrease in the overall size is mainly due to a collapse of the MANa corona and the formation of a second IPEC shell. Also, a decrease in the core size was observed hinting to a decrease in $N_{\text{agg.}}$ by ~25% (*cf.* eqn (1)) for BVqMANa$_{345}$ (2400 polymer chains per micelle) and ~45% for BVqMANa$_{465}$ (1700 polymer chains per micelle). This change in $N_{\text{agg.}}$ points towards a dynamic behavior of the micelles upon complex formation. The micrographs were further submitted to a grayscale analysis. This is exemplarily shown for the complex of BVqMANa$_{345}$ with Dq$_{820}$ at $Z_{+/-} = 0.5$ in Fig. 4.

Fig. 4A shows a single double-layered micellar IPEC particle. The rectangular black box shows the area used for the greyscale analysis in Fig. 4C. The different compartments of the micellar IPEC are depicted in the segments of the drawing in Fig. 4B. The B core exhibits a radius of 34.5 nm, and is surrounded by a thin, approx. 8 nm thick shell, resembling the former discontinuous *im*-IPEC shell of the precursor micelles. The newly formed IPEC shell, consisting of MANa and Dq, has a thickness of roughly 23 nm. As a $Z_{+/-}$ ratio of 0.5 was used, an uncomplexed MANa corona should emanate from the micellar IPEC. This is schematically shown in Fig. 4B with a blue/white gradient and is not distinguishable in the cryo-TEM image. However, as many of the micelles can be found closely agglomerated, the repelling effect of any uncomplexed and, hence, still charged MANa seems to be negligible. The numbers shown in Fig. 4C correspond to the different micellar compartments, also illustrated in Fig. 4A. Ideally, the greyscale analysis of the double-layered IPEC should be completely symmetrical. However, as the enlarged micellar aggregate was not located right in the centre of the cryo-TEM image taken, the electron beam intensity is slightly decreasing from the lower right to the upper left corner of Fig. 4A.

Addition of EO$_{325}$Dq$_{157}$ diblock copolymers to BVqMANa$_x$ micelles

If a double-hydrophilic block copolymer with one charged block (Dq) is used to generate core–shell–shell–corona structures from
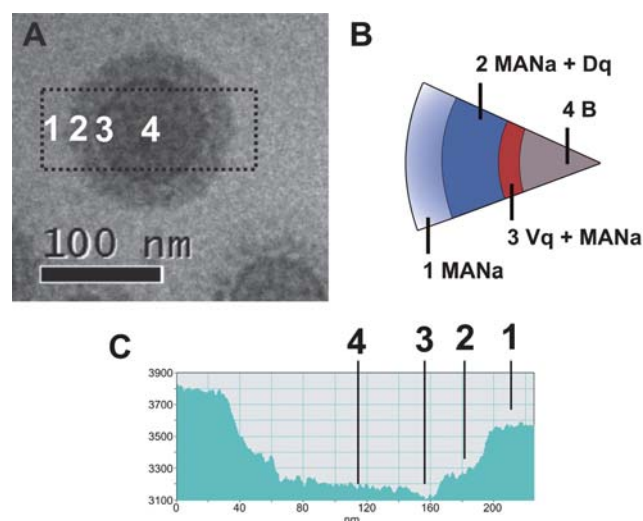

Fig. 4 Cryo-TEM micrograph of a single micellar IPEC of BVqMANa$_{345}$ and Dq$_{820}$ at $Z_{+/-} = 0.5$; the black box highlights the area used for the greyscale analysis (A); circle segment showing the four different regions revealed *via* grayscale analysis (B); greyscale analysis of the particle in (A), the numbers correspond to the respective areas (C).

different BVqMANa$_x$ precursor micelles, similar structures are supposed to form as shown earlier for Dq homopolymers. The only difference is that the other water-soluble block, EO, will serve as a solubilizing corona and, thus, further stabilize the resulting micellar IPECs. The micellar solutions were mixed with EO$_{325}$Dq$_{157}$ at different $Z_{+/-}$ ratios. Exemplarily, the DLS CONTIN plots for BVqMANa$_{345}$ and BVqMANa$_{465}$ at different $Z_{+/-}$ values are shown in Fig. 5.

For an easier comparison, the results from the DLS measurements of all micellar complexes prepared using EO$_{325}$Dq$_{157}$ as the cationically charged part are also summarized in Table 5.

In general, two things are expected to happen when EO$_{325}$Dq$_{157}$ is added to solutions of BVqMANa$_x$ precursor micelles: first, the complexation between MANa and Dq results in a corona contraction, like it was described above for the addition of Dq homopolymers at different $Z_{+/-}$ ratios; second, the EO compartment forms a new corona of the IPEC particles, stabilizing them in solution. The contraction of the former corona should be accompanied by a decrease in R_{h} whereas the new EO corona should have the opposite effect. As can be seen from Fig. 5 and the data in Table 5, for BVqMANa$_{345}$ and BVqMANa$_{465}$ a very slight increase in R_{h} can be observed for $Z_{+/-} = 0.5$ (170 to 184 nm and 146 to 147 nm). This might

indicate that the corona contraction is almost completely compensated by the addition of a new corona-forming block, EO. Surprisingly, in both cases larger size distributions are found in DLS measurements if $Z_{+/-}$ approaches unity. This can be seen in the CONTIN plots in Fig. 5A and B, where a new population is formed with an $R_h > 600$ nm. Again, the behavior observed for complexes of BVqMANa$_{550}$ and EO$_{325}$Dq$_{157}$ is different: at first ($Z_{+/-} = 0.25$), they increase in size (88 to 129 nm). Aggregation, according to DLS, for this particular system already occurs at $Z_{+/-} = 0.5$. This remains puzzling, as a sterical stabilization of the complex micelles would be anticipated due to the EO chains of the corona. One possible explanation would be that the intensity of the larger size distribution (entries 3, 6, and 9 in Table 5) is overestimated in DLS measurements as was demonstrated by Shibayama et al. for multi-modal distributions of colloidal particles and polymers in solution.[38] Further, another distribution at low $R_h = 10$ nm appears. We assume that this represents another micellar population, as it would be too large for EO$_{325}$Dq$_{157}$ unimers. To further investigate this, cryo-TEM was performed on micellar IPECs of all three BVqMANa$_x$/EO$_{325}$Dq$_{157}$ combinations at a representative $Z_{+/-}$ value. The results are shown in Fig. 6.

In general, the observed structures are similar, as shown in Fig. 6A–C. In all images large, spherical objects with a grey core (B) and a thin, dark ring around the core (the former, patchy im-IPEC shell, Vq + MANa) are found. Both are surrounded by
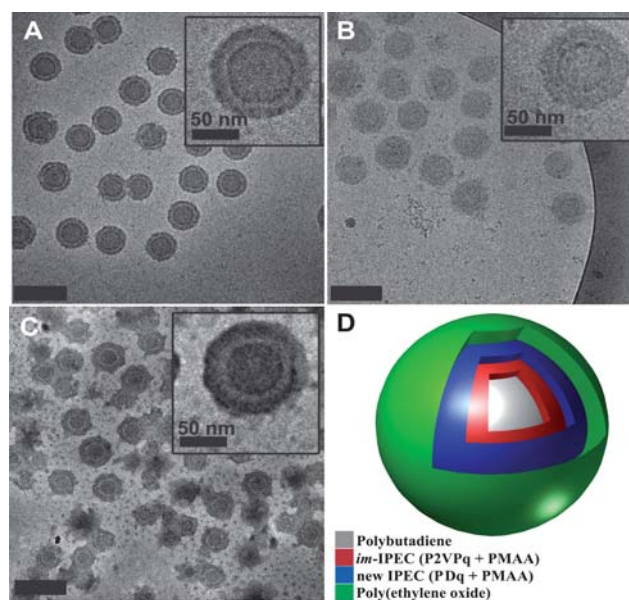

Fig. 6 Cryo-TEM images for micellar IPECs of BVqMANa$_{345}$/EO$_{325}$Dq$_{157}$ at $Z_{+/-} = 1.0$ (A); BVqMANa$_{465}$/EO$_{325}$Dq$_{157}$ at $Z_{+/-} = 1.0$ (B); BVqMANa$_{550}$/EO$_{325}$Dq$_{157}$ at $Z_{+/-} = 0.5$ (C); the insets in each part show a single double-layered particle at higher magnification; schematic depiction of the double-layered IPEC structure (D); all scalebars except for the insets correspond to 200 nm.
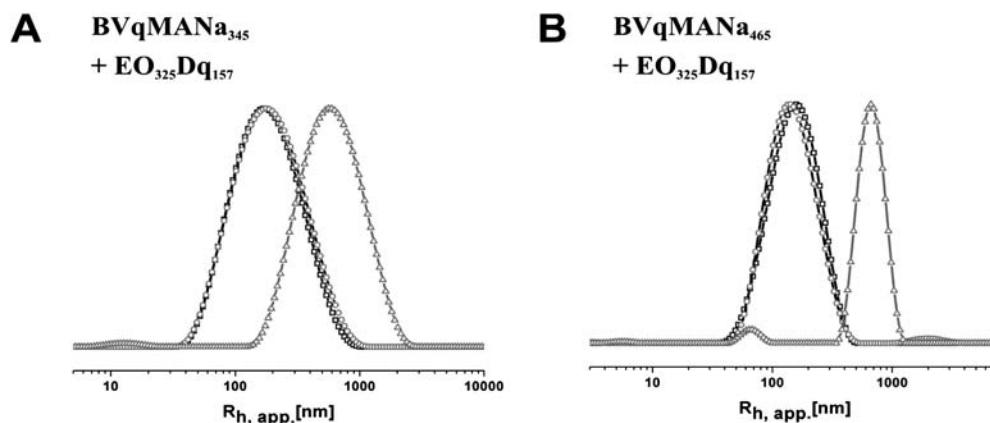

Fig. 5 DLS CONTIN plots for BVqMANa$_{345}$ (-□-, black), and micellar IPECs with EO$_{325}$Dq$_{157}$ at $Z_{+/-} = 0.5$ (-○-, grey), and 1.0 (-△-, grey) (A); BVqMANa$_{465}$ (-□-, black), and micellar IPECs with EO$_{325}$Dq$_{157}$ at $Z_{+/-} = 0.5$ (-○-, grey), and 1.0 (-△-, grey) (B).

Table 5 Solution characteristics of double-layered micellar IPECs prepared from BVqMANa$_x$ block terpolymer micelles and EO$_{325}$Dq$_{157}$ block copolymers

Entry	Sample	$Z_{+/-}$[a]	$\langle R_h \rangle_{z,app.}$[b]	PDI[c]
1	BVqMANa$_{345}$	—	170	0.18
2	BVqMANa$_{345}$ + EO$_{325}$Dq$_{157}$	0.5	184	0.28
3	BVqMANa$_{345}$ + EO$_{325}$Dq$_{157}$	1.0	11; 610	—
4	BVqMANa$_{465}$	—	146	0.21
5	BVqMANa$_{465}$ + EO$_{325}$Dq$_{157}$	0.5	147	0.20
6	BVqMANa$_{465}$ + EO$_{325}$Dq$_{157}$	1.0	6; 57; 660	—
7	BVqMANa$_{550}$	—	88	0.05
8	BVqMANa$_{550}$ + EO$_{325}$Dq$_{157}$	0.25	129	0.17
9	BVqMANa$_{550}$ + EO$_{325}$Dq$_{157}$	0.5	10; 104; 1300	—

[a] Ratio of added positive to remaining negative charges. [b] Determined via DLS. [c] Determined via cumulant analysis, if applicable.
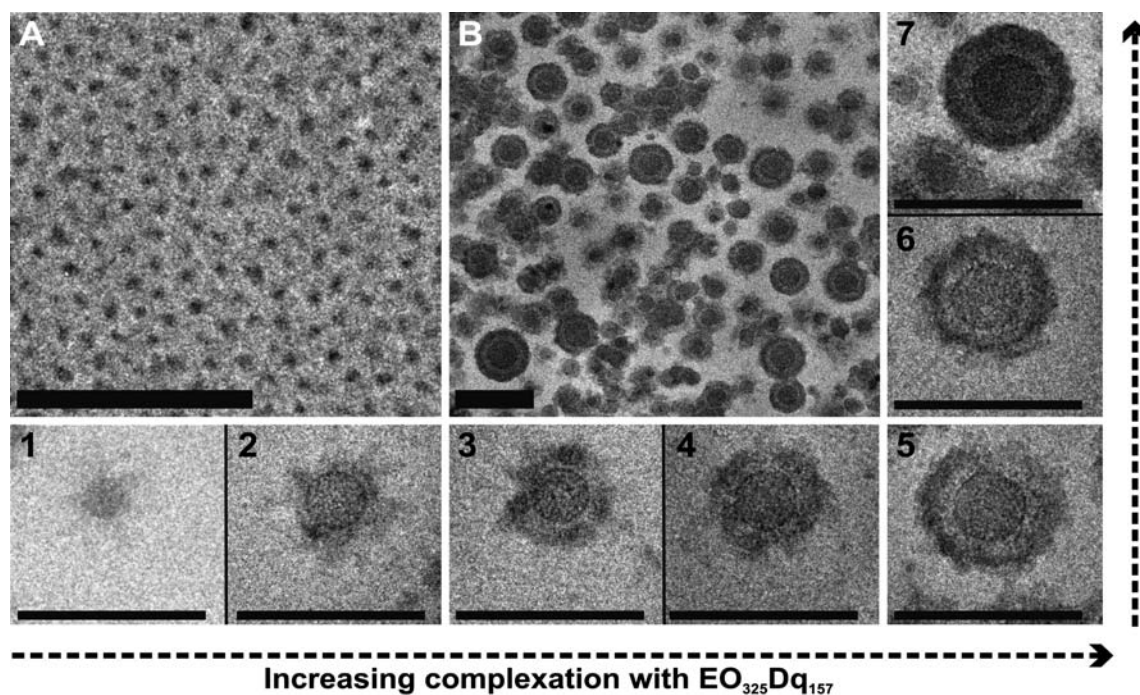
Fig. 7 Cryo-TEM images of smaller aggregates formed for BVqMANa$_{550}$/EO$_{325}$Dq$_{157}$ micellar IPECs at $Z_{+/-}$ = 0.5 (A); BVqMANa$_{550}$/EO$_{325}$Dq$_{157}$ at $Z_{+/-}$ = 0.25 (B); the small micrographs (1–7, all were taken from the same sample) depict single micellar IPECs at different stages of complexation with EO$_{325}$Dq$_{157}$; all scalebars correspond to 200 nm.

a lighter grey shell, followed by the newly formed second IPEC shell, appearing dark grey. The complex micelles of BVqMANa$_{345}$ and BVqMANa$_{465}$ show a rather homogeneous distribution, whilst BVqMANa$_{550}$ exhibits complexes at different stages of IPEC formation. For all three samples the double-layered character can be nicely confirmed. This is also shown in the three insets in Fig. 6A–C, each depicting a single IPEC particle. In the case of BVqMANa$_{465}$/EO$_{325}$Dq$_{157}$ (Fig. 6B), the distinction between the different shells is less pronounced than for the other two combinations. This could be due to ice-crystals that formed during the rapid vitrification of the sample for cryo-TEM measurement. Further, in Fig. 6C (BVqMANa$_{550}$/EO$_{325}$Dq$_{157}$), small dark dots can be seen. These aggregates exhibit an average core diameter of around 12 nm. This is far too small to refer to any of the used precursor micelles and could possibly represent the smallest distribution which was observed during DLS measurements. We tentatively try to explain this rather puzzling fact through aggregate formation from excess EO$_{325}$Dq$_{157}$. However, the driving force for such a behavior at the relatively low $Z_{+/-}$ value of 0.5 remains elusive. An alternative was to use a lower $Z_{+/-}$ ratio of 0.25. In this case, no such aggregates were found (Fig. 7B, for the DLS data also see Table 5, entries 2, 5 and 8).

Fig. 7A shows the small aggregates formed for BVqMANa$_{550}$/EO$_{325}$Dq$_{157}$ at $Z_{+/-}$ = 0.5. If the amount of added EO$_{325}$Dq$_{157}$ is reduced ($Z_{+/-}$ = 0.25, Fig. 7B), micellar IPECs at different stages of complexation are found, which is consistent with the increase in PDI as observed by DLS (Table 5, entries 7 and 8). We show a variety of examples, all found within the same cryo-TEM sample, shown in small micrographs 1–7 in Fig. 7; micrograph 1 depicts a precursor micelle of BVqMANa$_{550}$ (this was rather exceptional), and 2–6 then highlight different degrees of

complexation and 2nd IPEC shell formation. We believe that these structures represent non-equilibrium aggregates.

As already shown for the complexes with Dq homopolymers, the sizes of the individual compartments were estimated from the cryo-TEM images. The results are summarized in Table 6. It should be noted that, although for all three samples shown in Fig. 6A–C hydrodynamic radii distributions of several hundred nm were found in DLS, structures of such dimensions were never observed during cryo-TEM. We therefore ascribe the DLS results again to a certain clustering of the micellar IPECs in solution.

According to the image analysis, the overall radius of all micellar IPECs after complexation reaches a value of around 60 nm, when EO$_{325}$Dq$_{157}$ is used for the formation of the outer IPEC shell. However, the size of the individual compartments does vary significantly. As already observed for the complexes with Dq homopolymers, the size of the B core decreases with increasing MANa block length ($N_{agg.}$ decreases), while the size of the outmost shell increases only marginally. Interestingly, here the size of the individual compartments is the same as for the Dq homopolymers within the experimental error. Compared to the precursor micelles, the size of the B core (and $N_{agg.}$, if estimated with eqn (2)) decreases by 8% (BVqMANa$_{345}$), 13.5% (BVqMANa$_{465}$), and 25%/31% (BVqMANa$_{550}$, $Z_{+/-}$ = 0.25/0.5), respectively. Both the decrease in size observed for the micellar core and the collapse of the corona through the complex formation were also observed for the Dq complexes described earlier. This again indicates that such micellar particles are dynamic and "adjust" to changes in the surrounding conditions, *i.e.* to the formation of the 2nd IPEC shell.

To our opinion the lighter grey shell, surrounding the former *im*-IPEC shell of the precursor micelles, resembles uncomplexed

Table 6 Average sizes determined for the individual compartments of BVqMANa$_x$/EO$_{325}$Dq$_{157}$ complexes as determined by analysis of the cryo-TEM images

Compartment	BVqMANa$_{345}$/nm	BVqMANa$_{345}$/EO$_{325}$Dq$_{157}$ ($Z_{+/-}$ = 1.0)/nm	BVqMANa$_{465}$/nm	BVqMANa$_{465}$/EO$_{325}$Dq$_{157}$ ($Z_{+/-}$ = 1.0)/nm	BVqMANa$_{550}$/nm	BVqMANa$_{550}$/EO$_{325}$Dq$_{157}$ ($Z_{+/-}$ = 0.25)/nm	BVqMANa$_{550}$/EO$_{325}$Dq$_{157}$ ($Z_{+/-}$ = 0.5)/nm
R_{Micelle}	79.$_5$ ± 7	62.$_5$ ± 7	93.$_5$ ± 8	64 ± 7	91 ± 11	60.$_5$ ± 8	61 ± 9
R_{Core}	38 ± 5	35 ± 3	37 ± 8	32 ± 5	33.$_5$ ± 4	25 ± 5	23 ± 5
$D_{im\text{-IPEC}}$	5 ± 2	7 ± 2	3 ± 1	7.$_5$ ± 2	4 ± 1	4.4 ± 1	5 ± 2
$D_{\text{corona/2}^{nd}\text{ IPEC shell}}$	40 ± 5	24 ± 3	52 ± 6	27 ± 3	53 ± 9	28 ± 5	28 ± 6
$N_{\text{agg.}}$[a]	3200	2500	3000	1900	2200	900	700

[a] Estimated with eqn (2).
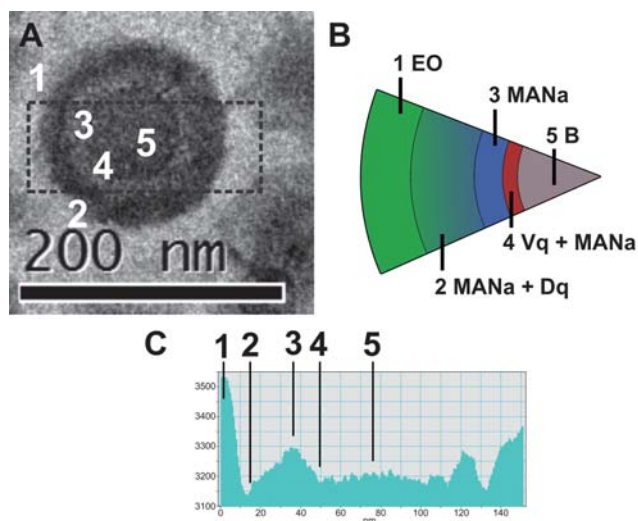
Fig. 8 Cryo-TEM image of a single micellar IPEC of BVqMANa$_{550}$/EO$_{325}$Dq$_{157}$ at $Z_{+/-}$ = 0.25; the black box highlights the area used for the greyscale analysis (A); circle segment showing the five different regions identified *via* greyscale analysis (B); greyscale analysis of the particle in (A), the numbers correspond to the respective areas (C).

MANa. Covering this MANa shell, a dark grey ring, presumably the newly formed IPEC between Dq and MANa, can be seen. To further evaluate the multi-layered character of these complex micelles, the micrographs were submitted to greyscale analysis. This is shown in Fig. 8.

A single double-layered IPEC micelle is shown in Fig. 8A. Clearly, two different shells around the soft B core are visible. The box drawn around the aggregate was used for the grey-scale analysis, which is shown in Fig. 8C. The grey-scale analysis identifies five different regions: region 1, with the lowest contrast, is the EO corona; 2, exhibiting the highest electron density, is presumably the newly formed IPEC between Dq and MANa; 3, uncomplexed MANa; 4, the formerly discontinuous shell of the BVqMANa$_x$ precursor micelles; and 5, the soft B core. The former patchy shell of the precursor micelles is rather thin with approx. 4 nm thickness. The newly formed shell(s) exhibit a combined thickness of around 28 nm. The core, with 50 nm diameter contracted, as compared to the precursor micelles in Fig. 1C. The different compartments of the micellar IPECs are also schematically depicted in the circle segment in Fig. 8B. Finally, the size of the surrounding EO corona cannot be estimated from the cryo-TEM micrographs as its electron density is

too low. Eventually, the greyscale analysis also confirms the existence of double-layered micellar IPECs at this stage.

Conclusions

We showed that by mixing of different negatively charged BVqMANa$_x$ block terpolymer precursor micelles with oppositely charged Dq or EO-b-Dq diblock copolymers in aqueous solution at pH 10 well-defined core–shell–shell–corona aggregates with two distinguishable IPEC shells can be prepared. We refer to these aggregates as double-layered IPECs, as both shells are formed as a result of the complexation between two oppositely charged polyelectrolytes. It turned out that the block terpolymer composition used for the preparation of the precursor micelles plays a crucial role as it affects the overall hydrophilic-to-hydrophobic balance of these aggregates.

If quaternized homopolymers (Dq) are used for the formation of the outer IPEC shell, stable micellar core–shell–shell–corona IPECs could be prepared up to a critical $Z_{+/-}$ ratio. Here, remaining uncomplexed MANa serves as the corona. Above that critical $Z_{+/-}$ value, further aggregation of the particles occurred. Further, under the rather dilute conditions reported here, the length of the added Dq was not observed to be crucial. If similar complexation reactions were performed using EO$_{325}$Dq$_{157}$ diblock copolymers, surprisingly, large aggregates were found above the same critical $Z_{+/-}$ ratios, although a water-soluble EO corona was formed. Additionally, in samples of BVqMANa$_{550}$ treated with the double-hydrophilic diblock copolymer above $Z_{+/-}$ = 0.25 small aggregates were observed in addition to the micellar IPECs, which we tentatively propose to consist of excess EO$_{325}$Dq$_{157}$. Overall, at optimized $Z_{+/-}$ ratios well-defined core–shell–shell–corona micellar IPECs were formed and the existence of a multi-layered structure was confirmed by cryo-TEM and greyscale analysis.

Some open questions remain: how does the dynamic character of the precursor micelles affect the formation of the outer IPEC layer? Can one make use of the different chemistries present in both adjacent IPEC shells? (We could already show that within the IPEC formed between MANa and Vq the formation of narrowly dispersed gold nanoparticles is possible.[27]) Why does a truly double-hydrophilic block copolymer, EO$_{325}$Dq$_{157}$, form aggregates in dilute aqueous solutions? We are currently pursuing these issues and hope to be able to address all points in further contributions.

Acknowledgements

References

1 G. Riess, *Prog. Polym. Sci.*, 2003, **28**, 1107–1170.
2 C. A. Fustin, V. Abetz and J. F. Gohy, *Eur. Phys. J. E*, 2005, **16**, 291–302.
3 M. Burkhardt, N. Martinez-Castro, S. Tea, M. Drechsler, I. Babin, I. Grishagin, R. Schweins, D. V. Pergushov, M. Gradzielski, A. B. Zezin and A. H. E. Müller, *Langmuir*, 2007, **23**, 12864–12874.
4 J. F. Gohy, N. Willet, S. Varshney, J.-X. Zhang and R. Jerome, *Angew. Chem., Int. Ed.*, 2001, **40**, 3214–3216.
5 X. Wang, G. Guerin, H. Wang, Y. Wang, I. Manners and M. A. Winnik, *Science*, 2007, **317**, 644–647.
6 T. Gädt, N. S. Ieong, G. Cambridge, M. A. Winnik and I. Manners, *Nat. Mater.*, 2009, **8**, 144–150.
7 H. Schmalz, J. Schmelz, M. Drechsler, J. Yuan, A. Walther, K. Schweimer and A. M. Mihut, *Macromolecules*, 2008, **41**, 3235–3242.
8 D. E. Discher and A. Eisenberg, *Science*, 2002, **297**, 967–973.
9 H. Cui, Z. Chen, S. Zhong, K. L. Wooley and D. J. Pochan, *Science*, 2007, **317**, 647–650.
10 Z. Li, M. A. Hillmyer and T. Lodge, *Langmuir*, 2006, **22**, 9409–9417.
11 G. Njikang, D. Han, J. Wang and G. Liu, *Macromolecules*, 2008, **41**, 9727–9735.
12 A. Walther, A. S. Goldmann, R. S. Yelamanchili, M. Drechsler, H. Schmalz, A. Eisenberg and A. H. E. Müller, *Macromolecules*, 2008, **41**, 3254–3260.
13 S.-C. Chen, S.-W. Kuo, C.-S. Liao and F.-C. Chang, *Macromolecules*, 2008, **41**, 8865–8876.
14 Z. Zhu, J. Xu, Y. Zhou, X. Jiang, S. P. Armes and S. Liu, *Macromolecules*, 2007, **40**, 6393–6400.
15 F. A. Plamper, J. R. McKee, A. Laukkanen, A. Nykänen, A. Walther, J. Ruokolainen, V. Aseyev and H. Tenhu, *Soft Matter*, 2009, **5**, 1812–1821.
16 A. Harada and K. Kataoka, *Science*, 1999, **283**, 65–67.
17 K. Kataoka, H. Togawa, A. Harada, K. Yasugi, T. Matsumoto and S. Katayose, *Macromolecules*, 1996, **29**, 8556–8557.
18 J. Koetz and S. Kosmella, *Polyelectrolytes and Nanoparticles*, Springer Verlag, Berlin, 2007.
19 K. S. Schanze and A. H. Shelton, *Langmuir*, 2009, **25**, 13698–13702.
20 V. A. Kabanov, *Russ. Chem. Rev.*, 2005, **74**, 3–20.
21 N. Lefevre, C. A. Fustin and J. F. Gohy, *Macromol. Rapid Commun.*, 2009, **30**, 1871–1888.
22 D. V. Pergushov, O. V. Borisov, A. B. Zezin and A. H. E. Müller, *Adv. Polym. Sci.*, DOI: 10.1007/12_2010_102.
23 P. S. Chelushkin, E. A. Lysenko, T. K. Bronich, A. Eisenberg, V. A. Kabanov and A. V. Kabanov, *J. Phys. Chem. B*, 2007, **111**, 8419–8425.
24 P. S. Chelushkin, E. A. Lysenko, T. K. Bronich, A. Eisenberg, V. A. Kabanov and A. V. Kabanov, *J. Phys. Chem. B*, 2008, **112**, 7732–7738.
25 M. Burkhardt, M. Ruppel, S. Tea, M. Drechsler, R. Schweins, D. V. Pergushov, M. Gradzielski, A. B. Zezin and A. H. E. Müller, *Langmuir*, 2008, **24**, 1769–1777.
26 D. V. Pergushov, E. V. Remizova, J. Feldthusen, A. B. Zezin, A. H. E. Müller and V. A. Kabanov, *J. Phys. Chem.*, 2003, **107**, 8093–8096.
27 F. Schacher, E. Betthausen, A. Walther, H. Schmalz, D. V. Pergushov and A. H. E. Müller, *ACS Nano*, 2009, **3**, 2095–2102.
28 F. Schacher, A. Walther and A. H. E. Müller, *Langmuir*, 2009, **25**, 10962–10969.
29 F. Schacher, J. Yuan, H. G. Schoberth and A. H. E. Müller, *Polymer*, 2010, **51**, 2021–2032.
30 F. Schacher, M. Müllner, H. Schmalz and A. H. E. Müller, *Macromol. Chem. Phys.*, 2009, **210**, 256–262.
31 F. A. Plamper, A. Schmalz, E. Penott-Chang, M. Drechsler, A. Jusufi, M. Ballauff and A. H. E. Müller, *Macromolecules*, 2007, **40**, 5689–5697.
32 F. Schacher, A. Walther, M. Ruppel, M. Drechsler and A. H. E. Müller, *Macromolecules*, 2009, **42**, 3540–3548.
33 A. Walther and A. H. E. Müller, *Chem. Commun.*, 2009, 1127–1129.
34 O. V. Borisov and E. B. Zhulina, *Macromolecules*, 2002, **35**, 4472–4480.
35 S. V. Larin, A. A. Darinskii, E. B. Zhulina and O. V. Borisov, *Langmuir*, 2009, **25**, 1915–1918.
36 L. Samokhina, M. Schrinner and M. Ballauff, *Langmuir*, 2007, **23**, 3615–3619.
37 D. V. Pergushov, I. A. Babin, F. A. Plamper, A. B. Zezin and A. H. E. Müller, *Langmuir*, 2008, **24**, 6414–6419.
38 M. Shibayama, T. Karino and S. Okabe, *Polymer*, 2006, **47**, 6446–6456.